Evans blue dye-enhanced capillary-resolution photoacoustic microscopy *in vivo*

Junjie Yao
Konstantin Maslov
Song Hu
Lihong V. Wang
Washington University in St. Louis
Optical Imaging Laboratory
Department of Biomedical Engineering
One Brookings Drive
St. Louis, Missouri 63130

Abstract. Complete and continuous imaging of microvascular networks is crucial for a wide variety of biomedical applications. Photoacoustic tomography can provide high resolution microvascular imaging using hemoglobin within red blood cells (RBCs) as an endogenic contrast agent. However, intermittent RBC flow in capillaries results in discontinuous and fragmentary capillary images. To overcome this problem, we use Evans blue (EB) dye as a contrast agent for *in vivo* photoacoustic imaging. EB has strong optical absorption and distributes uniformly in the blood stream by chemically binding to albumin. With the help of EB, complete and continuous microvascular networks—especially capillaries—are imaged. The diffusion dynamics of EB leaving the blood stream and the clearance dynamics of the EB-albumin complex are also quantitatively investigated. [DOI: 10.1117/1.3251044]

Keywords: photoacoustic imaging; Evans blue dye; diffusion dynamics; Evans blue-albumin clearance.

Paper 09184R received May 9, 2009; revised manuscript received Aug. 28, 2009; accepted for publication Sep. 2, 2009; published online Oct. 26, 2009.

1 Introduction

In the last decade, photoacoustic (PA) tomography, which combines the spatial resolution of ultrasound imaging with the contrast of optical absorption in deep biological tissues,[1,2] has gained great attention in biomedical applications.[3,4] Ultrasonic imaging yields better spatial resolution in deep tissues than optical techniques, because ultrasonic scattering is much weaker than optical scattering,[2] making possible image reconstruction based on propagated waves rather than energy diffusion. However, pure ultrasonic imaging is insensitive to early stage tumors and other biochemical properties, such as oxygen saturation or concentration of hemoglobin, because it is based on the detection of the bulk mechanical properties of biological tissues. By combining optical imaging with ultrasound, PA imaging can achieve both high contrast and high spatial resolution. PA imaging has been used for both structural and functional imaging of tumor,[5] brain cortex perfusion,[6,7] microvascular structure,[8] and hemoglobin concentration and oxygenation,[9] as well as for lymph flow cytometry.[10] Furthermore, it shows potential for blood flow measurement.[11,12] Since the amplitude of the PA signal is proportional to the absorbed optical energy density (i.e., specific optical absorption), the PA technique has the advantage of directly measuring the absorption spectra *in vivo*, allowing better tissue identification and providing functional information.[2,5,9,10] Thus PA imaging is complementary with other high resolution optical imaging modalities such as confocal microscopy, two-photon microscopy, and optical coherence tomography, which can provide *in vivo* imaging within the optical transport mean free path (~1 mm) of biological tissues.[13]

Previously, an optical-resolution confocal photoacoustic microscope (OR-PAM) was described, with a lateral resolution of 5 μm, axial resolution of 15 μm, and imaging depth greater than 0.7 mm.[8] OR-PAM is a good tool to image blood vessels at the capillary level. High spatial resolution of OR-PAM can resolve capillaries smaller than 10 μm in diameter[14] using hemoglobin within red blood cells (RBCs) as an endogenic contrast agent.

However, RBC flow in capillaries is discontinuous and changes greatly over time.[15–17] Because RBCs are the only noticeable optical absorbers in capillaries, it is highly likely that no absorber is present in a particular voxel during the laser pulse, which results in discontinuous capillaries in a RBC-based PA image. To acquire a complete capillary image and gain information about the capillary's functional state,[18] the use of an exogenic contrast agent is compelling.

In this work we use Evans blue (EB) dye for this purpose. EB has strong absorption in visible and near-infrared light, with a peak at 620 nm. EB is nontoxic and is used in measurement of blood volume,[19] lymph node location,[20] microvascular permeability,[21,22] blood-retinal barrier breakdown,[23] capillary perfusion,[17] and blood plasma flow,[15] among other applications. In the blood stream, EB mainly binds to serum albumin in a reversible manner, so it is uniformly distributed in the plasma, maximizing the chance to get a complete capillary network image. Under normal conditions, the EB-albumin (EBA) complex is confined to blood vessels, while the free dye more readily diffuses out into extravascular tissue. The diffused dye is bound to the surround-

Address all correspondence to: Lihong Wang, Dr., Optical Imaging Laboratory, Department of Biomedical Engineering, Washington University in St. Louis, One Brookings Dr., St. Louis, MO 63130. Tel: 314-935-6152; Fax: 314-935-7448; E-mail: lhwang@seas.wustl.edu

1083-3668/2009/14(5)/054049/6/$25.00 © 2009 SPIE

ing tissue proteins, and finally cleared out by either metabolism or excretion.[24–27]

This work seeks to achieve complete capillary network imaging, to quantitatively investigate the dynamic diffusion of EB out of the circulation system, and to elucidate the dynamic clearance of EBA.

2 Materials and Methods

2.1 *Optical-Resolution Confocal Photoacoustic Microscope System*

The OR-PAM system used in this work has been described in detail previously.[8] Briefly, a Nd:YLF laser (INNOSLAB, 523 nm, Edgewave, Aachen, Germany) pumped a dye laser (CBR-D, Sirah, Karst, Germany) used as the irradiation source. To cover the wavelength requirement for both RBCs and EB, laser dye Pyrro597 (peak at 582 nm, tuning range 566 to 611 nm) was employed. The ~7-ns laser pulse was passed through a 25-μm-diam pinhole and focused by a microscope objective lens (Olympus 4×, NA=0.1). The laser energy after the objective lens was ~100 nJ. Ultrasonic detection was achieved through a spherically focused ultrasonic transducer (V2012-BC, Panametrics-NDT, Olympus, focal spot size 27 μm) with a center frequency of 75 MHz, and a roundtrip 6-dB bandwidth of 80%, placed confocally with the optical objective. The PA signal detected by the ultrasonic transducer was amplified, digitized, and saved. The laser power was monitored by a reference channel to compensate for laser power instability. A volumetric image was generated by recording the time-resolved PA signal (A-line) at each horizontal location of the 2-D raster scan.

2.2 *Animal Preparation*

The ears of adult, 6- to 8-week-old nude mice (Hsd: Athymic Nude-Foxl^{NU} Harlan Company, Indianapolis, Indiana, body weight ~20 g) were used for all *in vivo* experiments here, because their small thickness allowed us to verify some of the PA results by using a standard bright field optical microscope. The nude mouse ear model has a well-developed vasculature and has been widely used to study tumor angiogenesis and other microvascular diseases.[28] Before data acquisition, the animal was anesthetized by an intraperitoneal injection of 85% ketamine and 15% xylazine (100-μl/g body weight). During data acquisition, the animal was placed on a warming pad (37 °C), and its head was held steady with a dental/hard palate fixture. The animal was kept still by using a breathing anesthesia system (E-Z Anesthesia, Euthanex, Palmer, Pennsylvania). After the experiment, the animal recovered naturally and was returned to its cage. All experimental animal procedures were carried out in conformity with the laboratory animal protocol approved by the Animal Studies Committee of the School of Medicine at Washington University in Saint Louis.

2.3 *Mode of Injection of Evans Blue*

A 6 or 3% EB w/v solution (Sigma, Saint Louis, Missouri) was prepared by dilution of the dye in phosphate-buffered saline (PBS, pH 7.5). Before injection, the solution was filtered through a 5-μm filter. An intravenous injection of EB was made to either of the dorsal veins of the tail. The injection lasted for about 10 to 20 s.

2.4 *Spatially Continuous Capillary Imaging Using Evans Blue as a Contrast Agent*

Two irradiation wavelengths 570 and 610 nm were chosen for RBC imaging and EB imaging, respectively. An area of 2×2 mm was chosen as the field of interest (FOI) near the margin of the nude mouse ear, where the capillary density was higher. Before the dye injection, control images were acquired with a scanning step size of 2.5 μm at 570 and 610 nm. The total scanning time for a complete volumetric dataset was ~30 min for each wavelength. To get sufficient imaging contrast and sensitivity of the capillaries, a relatively high concentration of EB in the blood plasma should be reached. Here 0.2 mL of 6% EB solution was injected in a nude mouse (body weight ~20 g). The total blood volume of the mouse was about 1.2 mL.[29] Thus the concentration of EB in the blood stream was ~1%, corresponding to an absorption coefficient of ~1000 cm^{-1} at 610 nm,[30] which is ~20 times higher than that of blood (~50 cm^{-1}). Two PA images at 610 nm were acquired, one immediately after the dye injection and the other 30 min later. Transmission optical microscopic images at 4× magnification were acquired before and after injection.

2.5 *Dynamics of Evans Blue Diffusion Out of the Blood Stream*

EB is removed from the vascular system principally by diffusing into extravascular tissue. At high dye concentrations, in the first few hours, it is mainly the free EB rather than the EB-albumin complex that diffuses out. The fixation of the free EB molecules by tissue proteins causes more dye to leave the blood to maintain chemical equilibrium, until the tissue proteins become saturated.[24–27,31] To better understand the diffusion dynamics, we monitored the dye diffusion over time and quantified the diffused dye volume in the tissue. Here, a smaller area of 1×1 mm was imaged near the margin of the nude mouse ear, so more datasets could be acquired over time due to the shorter scanning time of ~10 min. Control images at 570 nm 610 nm were acquired before dye injection. After 0.1 mL of 6% EB solution was injected, the dye molar concentration in the plasma was ~0.52 mM, which was a high concentration compared with the combination capability of albumin.[27] Right after injection, serial images at 610 nm were acquired every 20 min until the dye diffusion was observed to have reached saturation.

2.6 *Dynamics of the Evans Blue Albumin Clearance*

At low dye concentrations, EB exists almost exclusively in the form of EBA.[27] EB permeates wherever albumin is present. Therefore, the clearance dynamics of the EBA may be used to estimate the albumin metabolic rate in tissue.[27] To better understand the clearance dynamics, in our work the EBA volume in the tissue was monitored by PA imaging. An imaging area of 1×1 mm was chosen on the nude mouse ear, and control images at 570 and 610 nm were acquired before dye injection. Then 0.05 mL of 3% EB solution was injected

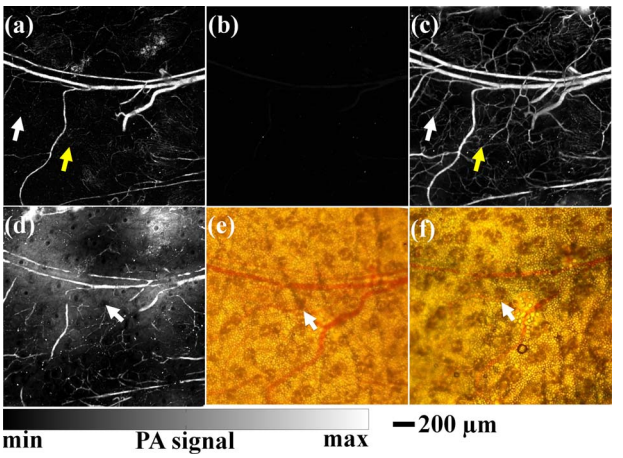

Fig. 1 EB enhanced photoacoustic imaging of mouse ear microvessels. PA microvascular image before dye injection acquired at (a) 570 nm and at (b) 610 nm. Arrows in (a) point to the fragmentary capillaries. (c) PA image acquired at 610 nm right after EB (6%, 0.2 mL) injection via tail vein. Arrows in (c) point to the continuous capillaries. (d) PA image acquired at 610 nm acquired 30 min after injection. Transmission microscopic images of the same area (e) before and (f) after injection. Arrows in (d), (e), and (f) point to sebaceous glands. All the photoacoustic images were scaled to the same level of PA signal.

via the tail vein. Serial images were acquired at 610 nm every one or two days, until EBA had almost completely cleared out.

2.7 *Quantitative Data Processing*

All the data processing in this work was based on the volumetric datasets. A typical 3-D data cube in this work consists of $200\times400\times400$ voxels for a 1×1-mm scanning area, or $200\times800\times800$ voxels for a 2×2-mm scanning area. Each voxel equals a physical size of $7.5\times2.5\times2.5$ μm. Hilbert transformation was performed along each A-line to extract the amplitude information. For visualization, a maximum amplitude projection (MAP) image was obtained by projecting the maximum value of each A-line onto the transverse scanning (x-y) plane. The EB or EBA volume was estimated by counting the voxels.

3 Results

3.1 *Spatially Continuous Capillary Imaging Using Evans Blue as a Contrast Agent*

In this study, EB solution (6%, 0.2 mL) was injected into the blood circulation system of the nude mouse. Before dye injection, a PA image was acquired at 570 nm [Fig. 1(a)]. Hemoglobin has strong absorption at this wavelength, which provided high imaging contrast and a high signal-to-noise ratio ($>$40 dB). Veins and arteries larger than 10 μm in diameter contained a higher area density of RBCs and appeared uniformly bright. However, smaller capillaries, containing a single of RBCs, looked discontinuous and fragmentary [see the arrows in Fig. 1(a)]. As a control, another image was acquired at 610 nm [Fig. 1(b)]. The signal was very weak due to the low hemoglobin absorption at 610 nm, which was only one-twentieth of that at 570 nm. Right after the dye injection,

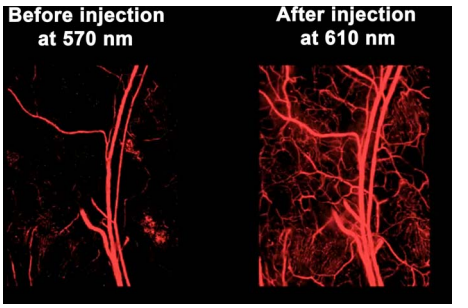

Video 1 A volumetric visualization of the images before dye injection at 570 nm and after dye injection at 610 nm (MOV, 0.9 MB). [URL: http://dx.doi.org/10.1117/1.3251044.1].

the microvascular network appeared continuous, as shown in Fig. 1(c). Dense capillaries could be observed, as indicated by arrows. All the capillaries that appear "broken" in Fig. 1(a) became smooth and continuous (Video 1). Moreover, the capillary branching points that were invisible in Fig. 1(a) could be clearly distinguished. The blood vessels in Fig. 1(c) appear somewhat thicker than those in Fig. 1(a), which was possibly because the plasma volume was larger than the RBC volume. The discernable blood vessel volume in the plasma-based image appeared to be more than 50% greater than that disclosed in the RBC-based image. The image in Fig. 1(d) was acquired at 610 nm 30 min after dye injection. It shows that a considerable amount of EB had diffused out of the blood vessels into the surrounding tissue but did not diffuse into the sebaceous glands, which appear as brown patches in the transmission microscopic images [see arrows in Figs. 1(d)–1(f)].

3.2 *Dynamics of Evans Blue Diffusion Out of the Blood Stream*

As before, control images at 570 and 610 nm were acquired before dye injection [Figs. 2(a) and 2(b)]. The whole microvascular network within the field of view showed up with denser and more continuous capillaries right after the 0.1 mL

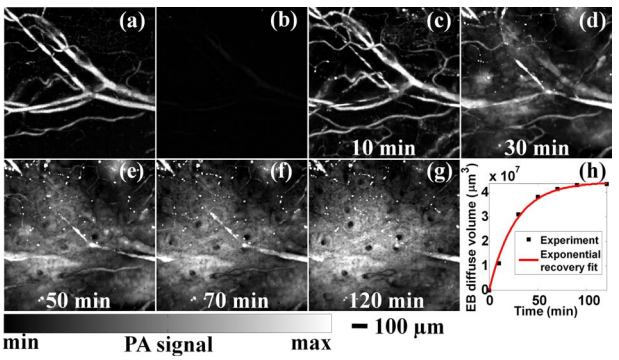

Fig. 2 Dynamics of EB diffusion out of the blood stream into surrounding tissue. PA images acquired before EB injection at (a) 570 nm and at (b) 610 nm (c) through (g) PA images acquired at 610 nm after EB (6%, 0.1 mL) injection at different times. (h) Partial volume of EB diffused into surrounding tissue. An exponential recovery model was used to fit the experiment data. All the photoacoustic images were scaled to the same level.

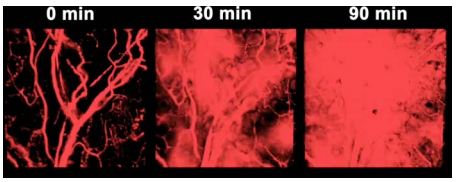

Video 2 A volumetric visualization of the dynamics of EB diffusion at 610 nm (QuickTime, 0.9 MB).
[URL: http://dx.doi.org/10.1117/1.3251044.2].

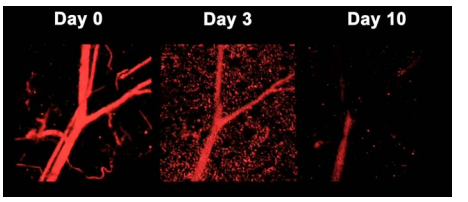

Video 3 A volumetric visualization of the dynamics of EBA clearance at 610 nm (QuickTime, 0.9 MB).
[URL: http://dx.doi.org/10.1117/1.3251044.3].

of 6% EB solution was injected [Fig. 2(c)]. Sequential images were acquired at different time points from 30 to 120 min [Figs. 2(d)–2(g); Video 2]. The partial volume of the free EB molecule diffused into extravascular tissue increased gradually and reached a plateau after ~2 h. If the dye left the blood vessels in a passive diffusion pattern, the extravascular dye volume could be fitted by an exponential recovery model.[32]

$$Q_T(t) = Q_e[1 - \exp(-kt)], \tag{1}$$

where $Q_T(t)$ and Q_e are the dye volumes at time t and equilibrium, respectively, and k is the dye diffusion rate. The fit result shows that EB indeed diffused in a passive pattern [Fig. 2(h)]. However, EB did not diffuse into the sebaceous glands, so more and more dark cavities were formed as the diffusion went on. Blood vessels were embedded in the diffused dye and capillaries became nearly invisible.

3.3 *Dynamics of Evans Blue Albumin Clearance*

To study the EBA clearance *in vivo*, 0.05 mL of 3% EB solution was injected. Before dye injection, Fig. 3(a) was acquired at 610 nm as a control image. Figures 3(b)–3(i) were acquired on different days after dye injection (Video 3). The EBA volume out of the blood vessels was calculated. Quantified clearance is shown in Fig. 4. The EBA volume in the extravascular tissue reached maximum on day 3 and then decreased to the base line by day 10. A two-compartment model was used to fit the EBA volume in the extravascular tissue.

$$\frac{dQ_V}{dt} = -k_1 Q_V,$$

$$\frac{dQ_T}{dt} = k_1 Q_V - k_2 Q_T, \tag{2}$$

where Q_V and Q_T are the EBA volumes in the blood stream and extravascular tissue, respectively. k_1 is the diffusion rate of EBA from the blood stream into the extravascular tissue, and k_2 is the clearance rate of EBA in the tissue. The results were consistent with the standard histological studies of long term EBA decline.[31,33]

4 Discussion

In this work, we demonstrate the feasibility of using Evans blue dye as a contrast agent to enhance *in vivo* photoacoustic microvascular imaging. Complete and continuous microvascular networks, especially capillaries, were imaged with the contrast of EB. And to the best of our knowledge, it is the first time that PA imaging has been used to study the dynamics of EB diffusion and EBA clearance.

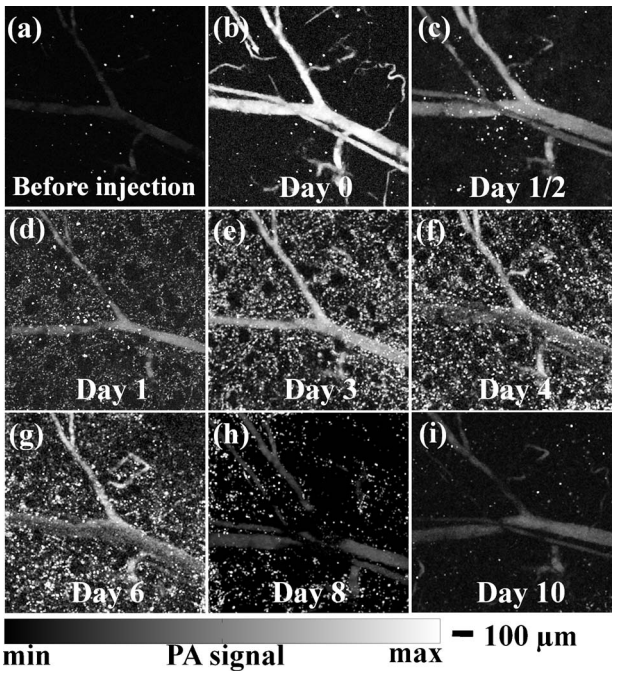

Fig. 3 Clearance dynamics of EBA. Before EB injection, (a) was acquired at 610 nm. On $\frac{1}{2}$ to 10 days following EB (3%, 0.05 mL) injection, images (b) through (i) were acquired at 610 nm. All the photoacoustic images were scaled to the same level.

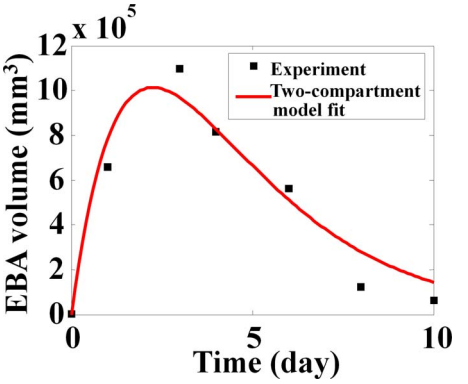

Fig. 4 Quantitative analysis of EBA clearance. After EB (3%, 0.05 mL) injection, the diffused EBA volume in the surrounding tissue reached maximum on day 3, and decayed to the baseline by day 10. A two-compartment model was used to fit the experiment data.

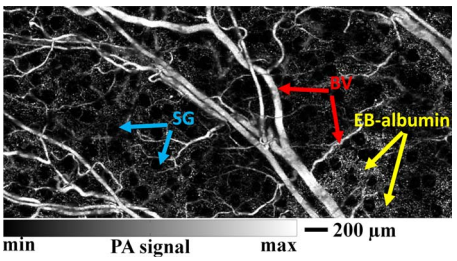

Fig. 5 Imaging sensitivity when a low concentration of EB was used. The image was acquired at 570 nm on day 2 after 0.02 mL of 0.3% EB solution was injected. BV is the blood vessel and SG is the sebaceous gland.

The photobleaching of EB may be crucial for quantitative study. In a previous study,[30] for a pulsed Nd:YAG laser (532 nm, 50 Hz, 14-ns pulse) and static 0.3% EB solution, photobleaching started after 1-min irradiation with an energy deposition of 20 mJ/pulse cm^2. In our study, the energy pulse deposition was about 100 mJ/pulse cm^2. However, the irradiation time was only 7 ns at each imaging position, which is much shorter than the reported photobleaching exposure time. Therefore, the influence of photobleaching on the quantitative study can be ignored, and the possibility that the apparent clearance of the dye was caused by photobleaching can be excluded.

At high EB concentrations, it is mainly the free dye that passively diffuses out of the blood vessels over tens of minutes. At low EB concentrations, as in most biological applications,[15,20,22,33,34] it is mainly the EBA that diffuses out of the blood vessels, and thus it is usually used as an indicator of the vessel leakage level. Our study was implemented under baseline conditions, where the blood vessel was leakage resistant for albumin, so relatively high EB concentrations were used here to study the dynamics. However, a high contrast PA image does not depend on whether free EB dye or EBA caused dye diffusion into extravascular tissue. The key point here is that the potential application of PA imaging combined with EB for physiological and pathological studies has been well demonstrated. Moreover, to test the imaging sensitivity, a commonly used EB injection dose (30-mg/kg body weight) was used (Fig. 5, Video 4). The diffused EBA can be clearly observed due to the high absorption contrast between the dye-protein complex and background tissue, hence the imaging sensitivity is sufficient for the biological applications.

It is interesting that EB and EBA did not diffuse into the sebaceous glands, where dark cavities were formed in the PA images, possibly caused by the denser structure or the biochemical properties of the sebaceous glands. The physiological characteristics of sebaceous glands have been thoroughly studied.[35] PA imaging facilitated by EB can provide 3-D structural and functional information of sebaceous glands, which are very important growth indexes during carcinoma development.

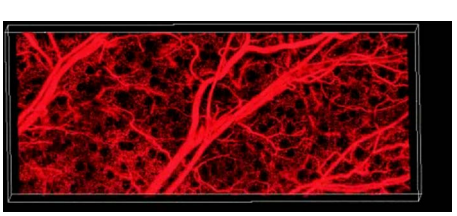

Video 4 A volumetric visualization of the image by using low concentration EB (QuickTime, 1.4 MB).
[URL: http://dx.doi.org/10.1117/1.3251044.4].

Acknowledgments

This research is supported by the National Institutes of Health grants R01 EB000712, R01 NS46214, R01 EB008085, and U54 CA136398. Author Wang has a financial interest in Endra, Incorporated, which, however, did not support this work.

References

1. M. H. Xu and L. H. V. Wang, "Photoacoustic imaging in biomedicine," *Rev. Sci. Instrum.* **77**(4), 041101 (2006).
2. H. F. Zhang, K. Maslov, G. Stoica, and L. H. V. Wang, "Functional photoacoustic microscopy for high-resolution and noninvasive *in vivo* imaging," *Nat. Biotechnol.* **24**(7), 848–851 (2006).
3. L. V. Wang, "Tutorial on photoacoustic microscopy and computed tomography," *IEEE J. Sel. Top. Quantum Electron.* **14**(1), 171–179 (2008).
4. L. V. Wang, "Prospects of photoacoustic tomography," *Med. Phys.* **35**(12), 5758–5767 (2008).
5. M. L. Li, J. T. Oh, X. Y. Xie, G. Ku, W. Wang, C. Li, G. Lungu, G. Stoica, and L. V. Wang, "Simultaneous molecular and hypoxia imaging of brain tumors *in vivo* using spectroscopic photoacoustic tomography," *Proc. IEEE* **96**(3), 481–489 (2008).
6. S. H. Yang, D. Xing, Y. Q. Lao, D. W. Yang, L. M. Zeng, L. Z. Xiang, and W. R. Chen, "Noninvasive monitoring of traumatic brain injury and post-traumatic rehabilitation with laser-induced photoacoustic imaging," *Appl. Phys. Lett.* **90**(24), 243902 (2007).
7. X. M. Yang and L. V. Wang, "Monkey brain cortex imaging by photoacoustic tomography," *J. Biomed. Opt.* **13**(4), 044009 (2008).
8. K. Maslov, H. F. Zhang, S. Hu, and L. V. Wang, "Optical-resolution photoacoustic microscopy for *in vivo* imaging of single capillaries," *Opt. Lett.* **33**(9), 929–931 (2008).
9. X. D. Wang, X. Y. Xie, G. N. Ku, and L. H. V. Wang, "Noninvasive imaging of hemoglobin concentration and oxygenation in the rat brain using high-resolution photoacoustic tomography," *J. Biomed. Opt.* **11**(2), 024015 (2006).
10. E. I. Galanzha, E. V. Shashkov, V. V. Tuchin, and V. P. Zharov, "*In vivo* multispectral, multiparameter, photoacoustic lymph flow cytometry with natural cell focusing, label-free detection and multicolor nanoparticle probes," *Cytometry, Part A* **73A**(10), 884–894 (2008).
11. H. Fang, K. Maslov, and L. V. Wang, "Photoacoustic doppler flow measurement in optically scattering media," *Appl. Phys. Lett.* **91**(26), 264103 (2007).
12. H. Fang, K. Maslov, and L. V. Wang, "Photoacoustic doppler effect from flowing small light-absorbing particles," *Phys. Rev. Lett.* **99**(18), 184501 (2007).
13. L. V. Wang and H. I. Wu, *Biomedical Optics: Principles and Imaging*, Wiley-Interscience, Hoboken, New Jersey (2007).
14. S. Takatani and M. D. Graham, "Theoretical analysis of diffuse reflectance from a two-layer tissue model," *IEEE Trans. Biomed. Eng.* **BME-26**(12), 656–664 (1979).
15. R. Abounader, J. Vogel, and W. Kuschinsky, "Patterns of capillary plasma perfusion in brains of conscious rats during normocapnia and hypercapnia," *Circ. Res.* **76**(1), 120–126 (1995).
16. E. Chaigneau, M. Oheim, E. Audinat, and S. Charpak, "Two-photon imaging of capillary blood flow in olfactory bulb glomeruli," *Proc. Natl. Acad. Sci. U.S.A.* **100**(22), 13081–13086 (2003).
17. A. Villringer, A. Them, U. Lindauer, K. Einhaupl, and U. Dirnagl, "Capillary perfusion of the rat-brain cortex—an *in vivo* confocal microscopy study," *Circ. Res.* **75**(1), 55–62 (1994).
18. P. Carmeliet and R. K. Jain, "Angiogenesis in cancer and other diseases," *Nature (London)* **407**(6801), 249–257 (2000).
19. T. D. Poulsen, T. Klausen, J. P. Richalet, I. L. Kanstrup, N. Fogh-Andersen, and N. V. Olsen, "Plasma volume in acute hypoxia: comparison of a carbon monoxide rebreathing method and dye dilution with Evans' blue," *Eur. J. Appl. Physiol.* **77**(5), 457–461 (1998).

20. M. I. Harrell, B. M. Iritani, and A. Ruddell, "Lymph node mapping in the mouse," *J. Immunol. Methods* **332**(1–2), 170–174 (2008).
21. W. G. Roberts and G. E. Palade, "Increased microvascular permeability and endothelial fenestration induced by vascular endothelial growth-factor," *J. Cell. Sci.* **108**(6), 2369–2379 (1995).
22. C. E. Patterson, R. A. Rhoades, and J. G. N. Garcia, "Evans blue-dye as a marker of albumin clearance in cultured endothelial monolayer and isolated lung," *J. Appl. Physiol.* **72**(3), 865–873 (1992).
23. Q. W. Xu, T. Qaum, and A. P. Adamis, "Sensitive blood-retinal barrier breakdown quantitation using evans blue," *Invest. Ophthalmol. Visual Sci.* **42**(3), 789–794 (2001).
24. M. I. Gregersen and R. A. Rawson, "The disappearance of t-1824 and structurally related dyes from the blood stream," *Am. J. Physiol.* **138**(5), 698–707 (1943).
25. R. A. Rawson, "The binding of t-1824 and structurally related diazo dyes by the plasma proteins," *Am. J. Physiol.* **138**(5), 708–717 (1943).
26. I. M. Klotz, F. M. Walker, and R. B. Pivan, "The binding of organic ions by proteins1," *J. Am. Chem. Soc.* **68**(8), 1486–1490 (1946).
27. H. H. LeVeen and W. H. Fishman, "Combination of evans blue with plasma protein: Its significance in capillary permeability studies, blood dye disappearance curves, and its use as a protein tag," *Am. J. Physiol.* **151**(1), 26–33 (1947).
28. S. Basu, J. A. Nagy, S. Pal, E. Vasile, I. A. Eckelhoefer, V. S. Bliss, E. J. Manseau, P. S. Dasgupta, H. F. Dvorak, and D. Mukhopadhyay, "The neurotransmitter dopamine inhibits angiogenesis induced by vascular permeability factor/vascular endothelial growth factor," *Nat. Med.* **7**(5), 569–574 (2001).
29. W. Sluiter, L. W. M. Oomens, A. Brand, and R. Vanfurth, "Determination of blood-volume in the mouse with chromium-51-labeled erythrocytes," *J. Immunol. Methods* **73**(1), 221–225 (1984).
30. M. C. Pilatou, E. Marani, F. F. M. de Mul, and W. Steenbergen, "Photoacoustic imaging of brain perfusion on albino rats by using evans blue as contrast agent," *Arch. Physiol. Biochem.* **111**(4), 389–397 (2003).
31. H. Sear, T. H. Allen, and M. I. Gregersen, "Simultaneous measurement in dogs of plasma volume with i131 human albumin and t-1824 with comparisons of their long term disappearance from the plasma," *Am. J. Physiol.* **175**(2), 240–242 (1953).
32. M. H. Wade, J. E. Trosko, and M. Schindler, "A fluorescence photobleaching assay of gap junction-mediated communication between human cells," *Science* **232**(4749), 525–528 (1986).
33. P. W. Hamer, J. M. McGeachie, M. J. Davies, and M. D. Grounds, "Evans blue dye as an *in vivo* marker of myofibre damage: optimising parameters for detecting initial myofibre membrane permeability," *J. Anat.* **200**(1), 69–79 (2002).
34. G. Thurston, C. Suri, K. Smith, J. McClain, T. N. Sato, G. D. Yancopoulos, and D. M. McDonald, "Leakage-resistant blood vessels in mice transgenically overexpressing angiopoietin-1," *Science* **286**(5449), 2511–2514 (1999).
35. A. J. Thody and S. Shuster, "Control and function of sebaceous glands," *Physiol. Rev.* **69**(2), 383–416 (1989).